Short-range antiferromagnetic correlations in high-T_c oxide superconductors

1996 J. Phys.: Condens. Matter 8 4411

(http://iopscience.iop.org/0953-8984/8/24/009)

J. Phys.: Condens. Matter **8** (1996) 4411–4428. Printed in the UK

Short-range antiferromagnetic correlations in high-T_c oxide superconductors

Arturo Marcello Allega†‡, Hideki Matsumoto‡ and Satoru Odashima‡

† Department of Theoretical Physics, University of Salerno, 84084 Baronissi (SA) and Ministero della Pubblica Istruzione, Italy

‡ Institute for Materials Research, Tohoku University, 980 Sendai, Japan

Received 4 October 1995, in final form 28 March 1996

Abstract. The modified Kondo–Heisenberg model for high-T_c oxide superconductors and the Kondo–Heisenberg model are analysed by the composite-operator expansion method. We study the effects of short-range antiferromagnetic correlations on the density of states and related band dispersion near the Fermi level when the Heisenberg insulator is doped. A set of self-consistent equations for fermionic correlation functions are solved by a numerical calculation. It turns out that the next-to-nearest-neighbour copper spin–spin correlations on extended lattice clusters can be used to predict the width of the band crossing the Fermi level in the same experimental range. Results are compared with previous calculations and a detailed discussion is given on the approximations implemented.

1. Introduction

High-T_c oxide superconductors have very peculiar properties [1] at the insulator–metal transition (IMT).

One way to investigate the IMT is by doping an antiferromagnetic spin background with a finite density of holes. Hole motion into a Heisenberg antiferromagnet is a long-standing stimulating problem [2-14]. Most interest, in the past, has been in the t–J model [2–5, 13, 14] analysed by spin-wave expansions [2, 13, 14], the slave-fermion Schwinger boson representation for Green functions [3, 4], and a string picture [5] for a variational wave function with the aim of achieving an understanding of the low-energy spectrum for Mott–Hubbard gap systems. Kondo–Heisenberg models have been derived [6–8] for charge-transfer gap models at the spin-fermion weak-coupling [6] and strong-coupling [7, 8] limits, and analysed by exact diagonalization [9], the projection operator method [10], and the composite-operator method [8, 11, 12]. Since the beginning, the first kind of approximation has been to consider the one-hole or at most the two-hole motion in the spin background [9, 10, 4], but just in the last few years calculations have been performed for finite-density hole motion into the spin-fluctuating background [3, 6–8, 11–14] at finite temperature.

On the other hand, frustration models [15–17] for spin–spin correlations have been introduced to provide the first theoretical picture of the phase diagram [15] for high-T_c superconductors. On the grounds of these models, it has been pointed out [15, 16] that spin-frustration mechanisms may lie behind the new phenomena. Moreover, it has also been stressed [18] that antiferromagnetic correlations up to second-order spin–spin correlations are needed even in the normal phase. Complicated configurations have been analysed for magnetic interactions [2–10, 13–16, 18–20], but up to now not beyond the strictly

0953-8984/96/244411+18$19.50

inner CuO_2 cluster correlations. Here, we show that, at second order of spin correlations, frustration turns out to be an important tool for estimating band-structure details of the models involved.

Recently, it has been shown [19, 20] that the p–d or Emery model [21] describes very well the main electronic excitations exhibited by the density of states (DOS) using two similar but different approaches: the projection operator method [19] and the composite-operator expansion method [20]. It is worth noting that in the two approaches almost the same collective excitations have been chosen to form the reduced Hilbert space for the operator expansion, and that slight differences do not affect the qualitative features of the results. However, neither calculation can predict the bandwidth (ΔW_s) of the p band of singlet character (W_s), which at moderate doping crosses the Fermi level, or the expected qualitative variation of the bandwidth ΔW_s with short-range spin fluctuations *and* doping. In [19] it is suggested that ΔW_s does not reduce to the experimental value [22] because short-range antiferromagnetic correlations are not taken into account up to the right order of magnitude, while in [20] it has been pointed out that the p–d mixing induces a triplet DOS transfer to the W_s-band that is too strong at the first-order level of the calculation.

In this paper we go a step further by concentrating on higher-order antiferromagnetic spin–spin correlations in the composite-operator expansion method [23, 20, 24, 12] for the following two models. To contain the amount of calculation and to study in detail the spin content of the p–d charge-transfer gap model, we consider its modified Kondo–Heisenberg (MKH) [8] spin-effective model version, for finite-density hole motion into the spin background at finite temperature. To understand the effect of the extended spin–spin interaction of Kondo type on a lattice cluster with respect to the standard on-site one on the spectral density of states (DOS) and the related band dispersion, we compare the MKH results to those given by the Kondo–Heisenberg (KH) model obtained from the MKH by restricting the interaction between the localized copper spin and the oxygen conduction electron spin to the on-site fixed Cu one only. We obtain the right tendency of ΔW_s with doping, the prediction of the bandwidth in the experimental range and, most importantly, an explanation for the spin-frustration mechanism that is at the heart of the results. A short communication on the present results has been reported in [11], stressing the spin effect at the first order of spin–spin correlations also present in the p–d model [20].

In the next section, we write down the effective MKH Hamiltonian derived from the p–d mixing model on the CuO_2 plane, and the special case of the KH model. The electron propagators are obtained by use of the retarded Green's function in a compact form. In section 3, a self-consistent numerical calculation is performed to obtain the DOS and the momentum dependence of the band dispersion energies including the Van Hove singularity. The results and a discussion of the systematic changes of the DOS at the IMT that occur on doping will be presented for the two models. Finally, section 4 is devoted to concluding remarks.

2. MKH and KH models

We consider the MKH model derived in [8] from the p–d mixing model on the CuO_2 plane in the $U \to \infty$ limit:

$$H = \int \mathrm{d}x \left[\epsilon_p p^\dagger p - t p^\dagger (1 - \alpha(-\mathrm{i}\nabla)) p + J_k p_\gamma^\dagger \boldsymbol{\sigma} p_\gamma \boldsymbol{n} + \frac{1}{2} J_H \boldsymbol{n}^\alpha \cdot \boldsymbol{n} \right] \tag{2.1}$$

where p is for the oxygen electron, $\boldsymbol{n} = d^\dagger \boldsymbol{\sigma} d$ is for copper spin fluctuations and

$$p_\gamma(x) = \gamma(-\mathrm{i}\boldsymbol{\nabla}) p(x) \tag{2.2a}$$

$$n^{\alpha}(x) = \alpha(-\mathrm{i}\boldsymbol{\nabla})n(x) \tag{2.2b}$$

with

$$\gamma(\boldsymbol{k})^2 = \sin^2\left(k_x\frac{a}{2}\right) + \sin^2\left(k_y\frac{a}{2}\right) \tag{2.3a}$$

$$\alpha(\boldsymbol{k}) = \frac{1}{2}(\cos(k_x a) + \cos(k_y a)) \tag{2.3b}$$

and $\gamma(\boldsymbol{k})^2 = 1 - \alpha(\boldsymbol{k})$.

In the Hamiltonian (2.1) and hereafter, we use the spinor notation. γ is defined on the p unit cluster identified in (2.3*a*) by half of the unit lattice step a and α on the d unit cluster identified in (2.3*b*) by the whole unit lattice step a. The clusters (overlapping of unit clusters) are extended over many lattice unit lengths. The KH model is simply given by $\gamma = 1$ because the p–d interaction is only given when a p hole moves on the d site. ϵ_p is the p-level energy, $J_k \sim t \simeq 0.6$ eV and $J \simeq 0.025$ eV are good estimates from phenomenological values [6–10] where t is related to the p–d energy transfer t_0 (see appendix A), and J_K and $J_H = 4J$ are respectively the Kondo and Heisenberg couplings.

The $U \to \infty$ limit of the Emery model is the main approximation of the calculation. It ensures that the collective excitations for describing the DOS are strongly determined by the level transitions given in close proximity to the Fermi level. A detailed derivation of this approximation is given in appendix A where also the correspondence between p–d and MKH parameters is given.

The MKH model and related versions have been thoroughly discussed by several authors [6–10]. Equation (2.1) is slightly different from the Hamiltonian derived in [8] because of the restriction that only the p–d bonding orbital combination is considered. This is because we are interested in the interaction between the Cu-electron localized spin and the p-hole itinerant spin on the *extended* clusters, and the energy scales involved show how strong the itinerant character of the system is with respect to the antiferromagnetic local nature of the insulator limit given by the Heisenberg term [6–10]. Also we know [19, 20] that the d band is almost unchanged by hole doping and spin–spin correlations; therefore, in this paper, we concentrate on investigating, in much more detail, the conduction p band close to the Fermi level (see appendix A).

The analytical method that we follow is the composite-operator expansion method pioneered in [23] and then improved in [20, 24, 12]. A summary of the method is given in appendix B.

We chose the following reduced Hilbert space (RHS) basis for composite operators in the MKH model:

$$\begin{pmatrix}\psi_1\\ \psi_2\end{pmatrix} = \begin{pmatrix}p_\gamma\\ p_s\end{pmatrix} \tag{2.4a}$$

where we use the notation

$$p_s = \boldsymbol{\sigma} p_\gamma \boldsymbol{n} \tag{2.4b}$$

which represents the conduction p electron dressed by copper spin fluctuations $\boldsymbol{n} = d^\dagger\boldsymbol{\sigma}d$. The equations of motion for ψ-fields are

$$\begin{aligned}
\mathrm{i}\frac{\partial}{\partial t}p_\gamma(x) &= (\epsilon_p - t)p_\gamma(x) + tp_\gamma^\alpha(x) + J_k\gamma^2(-\mathrm{i}\boldsymbol{\nabla})p_s(x)\\
\mathrm{i}\frac{\partial}{\partial t}p_s(x) &= 6J_k p_\gamma(x) + (\epsilon_p - t + 2J_k)p_s(x) + t\boldsymbol{\sigma}p_\gamma^\alpha(x)\boldsymbol{n}\\
&\quad + 2J_k\left(\boldsymbol{\sigma}p_\gamma(x)\boldsymbol{k} - \frac{1}{2}\lambda\boldsymbol{\sigma}p_\gamma^\alpha(x)\boldsymbol{n}\right) + 2J\boldsymbol{\sigma}p_\gamma(x)\boldsymbol{l}
\end{aligned} \tag{2.5}$$

where the high-order composite operators are

$$\begin{aligned} l_i &= \mathrm{i}\epsilon_{ijk} n_j^{\alpha} n_k \\ c_i &= p_{\gamma}^{\dagger} \sigma_i p_{\gamma} \\ k_i &= \mathrm{i}\epsilon_{ijk} c_j n_k. \end{aligned} \tag{2.6}$$

The operator l_i carries information on high-order Cu–Cu cluster spin correlations; the c_i-operator is proportional to the oxygen hole number; and k_i is for the conduction hole dressed by spin fluctuations.

The normalization matrix is defined by

$$(I(\boldsymbol{k}))_{nl} = \mathrm{FT}\langle\{\psi_n(\boldsymbol{x}), \psi_l^{\dagger}(\boldsymbol{y})\}\rangle \tag{2.7}$$

and therefore

$$I = \begin{pmatrix} 1 - \lambda\alpha & 0 \\ 0 & I_{ss} \end{pmatrix} \tag{2.8}$$

where $\langle ... \rangle$ indicates the thermal average and

$$I_{ss} = 3 + 4a_s - 3\lambda n'_{00}\alpha \tag{2.9}$$

with $a_s = \langle p_s p_{\gamma}^{\dagger} \rangle$ and $n'_{00} = \frac{1}{3}\langle \boldsymbol{n}\boldsymbol{n}^{\alpha} \rangle$. The parameter λ is present to select out, from now on, the KH model when $\lambda = 0$.

Any correlation function related to physical observables is calculated using the generalized retarded Green function or retarded propagator defined by

$$\mathrm{FT}\langle R\psi_n(x)\psi_l^{\dagger}(y)\rangle = \left(I(\boldsymbol{k}) \frac{1}{\omega I(\boldsymbol{k}) - (m(\boldsymbol{k}) + \delta m(\omega, \boldsymbol{k}))} I(\boldsymbol{k}) \right)_{nl} \tag{2.10a}$$

or

$$S(\omega, \boldsymbol{k}) = \left(\frac{1}{\omega - E(\omega, \boldsymbol{k}))} I(\boldsymbol{k}) \right)_{nl}. \tag{2.10b}$$

In a mean-field approximation we impose $\delta m(\omega, \boldsymbol{k}) = 0$ which restricts the dispersion energy of the band to being only $\boldsymbol{k}$-dependent: $E = E(\boldsymbol{k})$. This is the second approximation that we consider (see the conclusions in section 4).

The energy matrix E is given by

$$\begin{aligned} E_{00} &= m_{00} I_{00}^{-1} = \epsilon_p + t(1 - \alpha) \\ E_{0s} &= m_{0s} I_{ss}^{-1} = J_k(1 - \alpha) \\ E_{s0} &= m_{s0} I_{00}^{-1} = J_k I_{ss} \\ E_{ss} &= m_{ss} I_{ss}^{-1} \end{aligned} \tag{2.11}$$

and the mass matrix by

$$m = \begin{pmatrix} m_{00} & m_{0s} \\ m_{s0} & m_{ss} \end{pmatrix} \tag{2.12}$$

where

$$(m(\boldsymbol{k}))_{nl} = \mathrm{FT}\left\langle \left\{ \mathrm{i}\frac{\partial}{\partial t}\psi_n(\boldsymbol{x}), \psi_l^{\dagger}(\boldsymbol{y}) \right\} \right\rangle. \tag{2.13}$$

It is related to the generalized self-energy Σ by $m = \Sigma I$ (for details see appendix B). Explicitly the mass matrix elements are

$$\begin{aligned}
m_{00} &= [\epsilon_p - t(1-\alpha)]I_{00} \\
m_{0s} &= J_k I_{00} I_{ss} \\
m_{s0} &= m_{0s} \\
m_{ss} &= (\epsilon_p - t + 2J_k)I_{ss} + t\{4a'_s + 3n'_{00}\alpha - 3\lambda n''_{00}\alpha^2\} \\
&\quad - 4J_k\left\{(3a + 2a_s) + \lambda\left[\frac{3}{8}n'_{00}(4+\alpha)\alpha + 4a'_{ss} - 8C_{pna}a_{ss}\alpha\right]\right\} \\
&\quad + 4J\left(3n'_{00} + \frac{4}{3}a'_{ss}\alpha - 2C_{pna}a_{ss}\right) + \frac{3}{4}\lambda n'_{00}\alpha
\end{aligned} \tag{2.14}$$

where $a_{ss} = 2a_s + 3a$ with $a = \langle p_\gamma p^\dagger_\gamma\rangle$ the p-hole density in the Cu_2O cluster and $a_s = \langle p_s p^\dagger_\gamma\rangle$ the p-hole–d-spin correlation; moreover, we have $a'_s = \langle p^\alpha_s p^\dagger_\gamma\rangle$, $a'_{ss} = \langle p^\alpha_s p^\dagger_s\rangle$ for high-order p-hole–d-spin intersite (dashed) correlations, $n'_{00} = \langle \frac{1}{3}\boldsymbol{n}\boldsymbol{n}^\alpha\rangle$ for nearest-neighbour d-spin correlation, and $n''_{00} = \langle \frac{1}{3}\boldsymbol{n}^\alpha\boldsymbol{n}^\alpha\rangle$ for next-to-nearest-neighbour d-spin correlations.

Here, the coefficient C_{pna} is related to high-order fermionic mean fields given by [12]

$$C_{pna} = \frac{3}{2a_{ss}}n'_{00p} \equiv \frac{3}{2a_{ss}}\langle \mathrm{tr}(p_\gamma p^\dagger_\gamma)n^\alpha_l n_l\rangle.$$

We expand the higher-order composite operator $p_\gamma n^\alpha_l$ in terms of the operator basis (2.2) of the RHS by following the approximation of appendix A restricted to contributions around the Fermi level:

$$p_\gamma n^\alpha_l \simeq a_{pna}p_\gamma + b_{pna}p_s. \tag{2.15}$$

The expansion coefficients are determined by thermal average normalization of anticommutators:

$$\begin{aligned}
a_{pna} &= \langle\{p_\gamma n^\alpha_l, p^\dagger_\gamma\}\rangle = 0 \\
b_{pna} &= \langle\{p_\gamma n^\alpha_l, p^\dagger_s\}\rangle I^{-1}_{ss} = \frac{1}{3}C_{pna}\sigma_l
\end{aligned}$$

and by explicit calculation of $\langle\{p_\gamma n^\alpha_l, p^\dagger_s\}\rangle$ we have

$$C_{pna} = 3I^{-1}_{ss}\left[n'_{00} + \frac{4}{3}a'_s\alpha - \lambda n''_{00}\alpha\right]. \tag{2.16}$$

Finally, we have from (2.15)

$$\langle(p_\gamma p^\dagger_\gamma)n^\alpha_l n_l\rangle \simeq \left\langle\left(\frac{1}{3}C_{pna}\sigma_l p_s\right)(p_\gamma n^\alpha_l)\right\rangle = \frac{1}{3}C_{pna}a_{ss}.$$

The higher-order mean-field $\langle p_\gamma p^\dagger_\gamma n^\alpha_k n_l\rangle$ can be decomposed in the Pauli matrices basis as

$$\langle p_\gamma p^\dagger_\gamma n^\alpha_k n_l\rangle = \frac{1}{2}\{\delta_{km}\langle \mathrm{tr}(p_\gamma p^\dagger_\gamma)n^\alpha_l n_l\rangle - \sigma_q\langle c_q n^\alpha_k n_l\rangle\}$$

where $\langle c_q n^\alpha_k n_l\rangle$ is a chiral state which is neglected because of the assumption of a paramagnetic ground state.

Observe that we can also write the equations of motion in terms of the energy coefficients:

$$\mathrm{i}\frac{\partial}{\partial t}\psi(x) = \begin{pmatrix} E_{00} & E_{0s} \\ E_{s0} & E_{ss}\end{pmatrix}\psi. \tag{2.17}$$

In this way we see that the new states are given by energy level mixing among the *bare* states. By writing the determinant of the S-matrix explicitly, we identify two poles given by the following two energy eigenvalues:

$$E_{\pm}(\boldsymbol{k}) = \frac{1}{2}\left\{E_{ss} + E_{00} \pm \sqrt{(E_{ss} - E_{00})^2 + 4E_{0s}E_{s0}}\right\}(\boldsymbol{k}) \tag{2.18}$$

and therefore the dispersion energies of the two bands related to the two *composite quasiparticles* generated by the overlapping excitation modes from the fundamental fields p_γ and p_s. Finally, we have for the propagators

$$\begin{aligned}
S_{p_\gamma p_\gamma^\dagger} &= I_{00}\left[\frac{E_+ - E_{ss}}{E_+ - E_-}\frac{1}{\omega - E_+} - \frac{E_- - E_{ss}}{E_+ - E_-}\frac{1}{\omega - E_-}\right] \\
S_{p_s p_\gamma^\dagger} &= I_{00}\frac{E_{s0}}{E_+ - E_-}\left[\frac{1}{\omega - E_+} - \frac{1}{\omega - E_-}\right] \\
S_{p_s p_s^\dagger} &= I_{ss}\left[\frac{E_+ - E_{00}}{E_+ - E_-}\frac{1}{\omega - E_+} - \frac{E_- - E_{00}}{E_+ - E_-}\frac{1}{\omega - E_-}\right]
\end{aligned} \tag{2.19}$$

and any fermionic correlation function is calculated from the self-consistent integral equation

$$\langle\psi\psi^\dagger\rangle = \frac{1}{(2\pi)}\int \mathrm{d}\omega\ \sigma_{\psi\psi^\dagger}(\omega)(1 - f_F(\omega)) \tag{2.20a}$$

where

$$\sigma_{\psi\psi^\dagger}(\omega) = \frac{\Omega}{(2\pi)^2}\int \mathrm{d}^2k\ \left(-\frac{1}{\pi}\right)\mathrm{Im}\, S_{\psi\psi^\dagger}(\omega, \boldsymbol{k}) \tag{2.20b}$$

is the spectral function and $f_F(\omega)$ is the Fermi distribution function.

To select the KH model we only need to put $\gamma = 1$ and $\lambda = 0$ in all of the equations. By looking at the matrix elements of I and m we can observe that in the λ-terms we have n''_{00}-, α^2-, and a'_{ss}-contributions. The consequences of these high-order α-dependent contributions in the λ-terms will be discussed in the next section.

3. Numerical results for the MKH and KH models

Summarizing the above scheme, we list the complete set of parameters appearing in the self-consistent integral equations (2.20): $a = \langle p_\gamma p_\gamma^\dagger\rangle$ is the p-hole density in the Cu_2O cluster, $a_s = \langle p_s p_\gamma^\dagger\rangle$ is the p-hole–d-spin correlation, and $a'_s = \langle p_s^\alpha p_\gamma^\dagger\rangle$ and $a'_{ss} = \langle p_s^\alpha p_s^\dagger\rangle$ are the high-order p-hole–d-spin intersite (dashed) correlations; and the bosonic mean fields: $n'_{00} = \langle\frac{1}{3}\boldsymbol{n}\cdot\boldsymbol{n}^\alpha\rangle$ is the nearest-neighbour d-spin correlation, and $n''_{00} = \langle\frac{1}{3}\boldsymbol{n}^\alpha\cdot\boldsymbol{n}^\alpha\rangle$ is the next-to-nearest-neighbour d-spin correlation. High-order fermionic mean fields might be, generally, reduced to a combination of fermionic mean fields made up of the basis fields in the RHS and the above bosonic fields which derive from the Heisenberg term in the Hamiltonian (as was done for C_{pna}).

Up to now, we have only dealt with fermionic propagators; therefore the bosonic mean fields cannot be self-consistently calculated via the present approximation. We have been successful in ensuring the mathematical self-consistency in the Hubbard model while leaving out any free parameter [25, 26]. For MKH and KH models, we consider $n'_{00} = \langle\frac{1}{3}\boldsymbol{n}\boldsymbol{n}^\alpha\rangle$, $n''_{00} = \langle\frac{1}{3}\boldsymbol{n}^\alpha\boldsymbol{n}^\alpha\rangle$ as input parameters [20], and look at their effects on the fermionic observables. This approximation has been good enough to lead to a good qualitative DOS in the p–d model; therefore, we retain the same set-up as given for the p–d model in [20] to explore 'by hand' the physics of antiferromagnetic correlations. Of course, we look

upon the present results as very important check points for a more rigorous self-consistent calculation of both fermion and boson parameters.

After having found the convergent values for the fermionic unknowns, we calculate the DOS spectrum given by equation (2.20). In Kondo–Heisenberg-type models the bare level structure is given by the exact Kondo model with the following solution:

$$S_{pp^\dagger}(\omega) = \frac{1}{4}\frac{1}{\omega - (\epsilon_p + \frac{3}{2}J)} + \frac{3}{4}\frac{1}{\omega - (\epsilon_p - \frac{1}{2}J)}. \tag{3.1}$$

A singlet state with energy $\epsilon_p + \frac{3}{2}J$ and a triplet state with energy $\epsilon_p - \frac{1}{2}J$ are identified. The same solution [23] is obtained by the composite-operator method for a Kondo model with the RHS given by the basis (2.4*a*) with $\gamma = 1$ in equation (2.4*b*). Of course, in the MKH model, composite excitations are obtained by a mixing of the basic operators (2.4) or by a linear combination of p_γ and p_s (with $\gamma \neq 1$), as is shown by equation (2.17), and they correspond to a singlet Kondo-type band (SB) and a triplet Kondo-type band (TB) with shifted energy pole positions with respect to that of the pure Kondo model. These new energy positions must be compared with experiment to provide a good starting point for the analytical scheme. Band dispersion energies are given by equation (2.18) for the SB and for the TB respectively by E_+ and E_-.

Table 1. Calculated MKH mean fields for fixed hole number n_h and nearest-neighbour spin correlations n'_{00}. n''_{00} is fixed at $n''_{00} = 0.25$.

n_h (n'_{00})	0.01 (0.0)	0.1 (0.0)	0.01 (−0.2)	0.1 (−0.2)	0.01 (−0.4)	0.1 (−0.4)
ϵ_p	−0.9446	−0.8587	−0.7978	−0.7520	−0.7700	−0.6873
a	0.0095	0.0875	0.0063	0.0802	0.0044	0.0479
a_s	0.0208	0.1947	0.0152	0.1713	0.0127	0.1255
a'_s	−0.0189	−0.1476	−0.0042	−0.1069	0.0014	0.0043
a_{ss}	0.0701	0.6518	0.0492	0.5833	0.0386	0.3944
a'_{ss}	−0.0411	−0.3272	−0.0095	−0.2240	0.0045	0.0149
n'_{00p}	0.0000	0.0000	−0.0025	−0.0321	−0.0035	−0.0382

Table 2. Calculated MKH mean fields for fixed hole number n_h and nearest-neighbour spin correlations n'_{00}. n''_{00} is fixed at $n''_{00} = 0.4$.

n_h (n'_{00})	0.01 (0.0)	0.1 (0.0)	0.01 (−0.2)	0.1 (−0.2)	0.01 (−0.4)	0.1 (−0.4)
ϵ_p	−0.9050	−0.8510	−0.8130	−0.7394	−0.7882	−0.7027
a	0.0086	0.0869	0.006358	0.0647	0.0046	0.0487
a_s	0.0191	0.1912	0.0147	0.1511	0.0131	0.1281
a'_s	−0.0138	−0.1427	−0.0023	−0.0466	0.0010	0.0024
a_{ss}	0.0638	0.6429	0.0467	0.4963	0.0399	0.4024
a'_{ss}	−0.0304	−0.3122	−0.0056	−0.1048	0.0033	0.0094
n'_{00p}	0.0000	0.0000	−0.0023	−0.0259	−0.0037	−0.0390

$\boldsymbol{k}$-integration is simplified by the fact that $\boldsymbol{k}$-dependence appears only through $\alpha(\boldsymbol{k})$ (here note that $\gamma^2(\boldsymbol{k}) = 1 - \alpha(\boldsymbol{k})$), $\sigma_{\psi_n\psi_n^\dagger}(\omega, \boldsymbol{k})$ is given in the form $\sigma_{\psi_n\psi_n^\dagger}[\omega, \alpha(\boldsymbol{k})]$, and $\boldsymbol{k}$-integration can be performed to get the one-particle density of states [22]:

$$\sigma_{\psi_n\psi_n^\dagger}(\omega) = \frac{\Omega}{(2\pi)^2}\int \mathrm{d}^2k\ \sigma_{\psi_n\psi_n^\dagger}[\omega, \alpha(\boldsymbol{k})] \tag{3.2a}$$

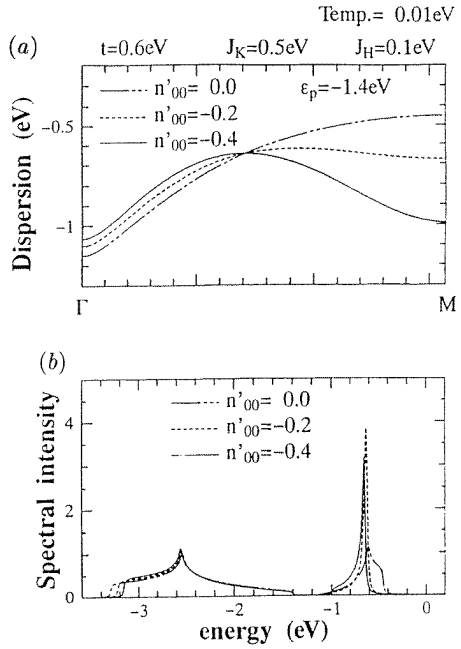

Figure 1. (*a*) The MKH dispersion energy $E_+(\boldsymbol{k})$ of the SB, and (*b*) the $\boldsymbol{k}$-integrated spectral density $\sigma_{pp}(\omega)$, both for the undoped regime ($n_h = 0$ at $\epsilon_p = -1.4$ eV) and for three n'_{00}-values: 0.0 (chain), -0.2 (dashed), -0.4 (line). The parameter n''_{00} is fixed at $n''_{00} = 0.25$. The temperature is $T = 0.01$ eV.

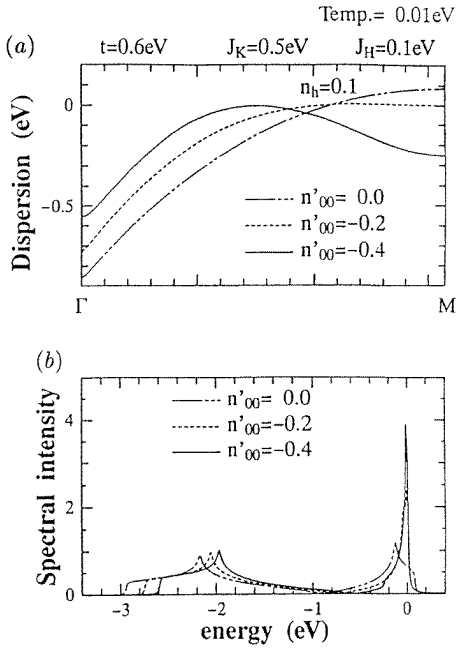

Figure 2. (*a*) The MKH dispersion energy $E_+(\boldsymbol{k})$ of the SB, and (*b*) the $\boldsymbol{k}$-integrated spectral density $\sigma_{pp}(\omega)$, both for the doped regime ($n_h = 0.1$) and for three n'_{00}-values: 0.0 (chain), -0.2 (dashed), -0.4 (line). The parameter n''_{00} is fixed at $n''_{00} = 0.25$. The temperature is $T = 0.01$ eV.

that is

$$\sigma_{\psi_n\psi_n^\dagger}(\omega) = \int \mathrm{d}\alpha \; w(\alpha)\sigma_{\psi_n\psi_n^\dagger}[\omega, \alpha] \tag{3.2b}$$

where the function $w(\alpha)$ is the elliptic integral of the first kind:

$$\begin{aligned} w(\alpha) &= \frac{\Omega}{(2\pi)^2}\int \mathrm{d}^2k \; \delta(\alpha - \alpha(\boldsymbol{k})) \\ w(\alpha) &= \frac{2}{\pi^2}K\left(\sqrt{1-\alpha^2}\right) \end{aligned} \tag{3.3}$$

and takes into account the Van Hove singularity.

In tables 1–3 we report the convergent data for fermionic calculated mean fields with the fixed parameters $t = 0.6$ eV, $J_k = 0.5$ eV, $J = 0.025$ eV and temperature $T = 0.01$ eV. Table 1 is for the MKH model for $n''_{00} = 0.25$ and table 2 is for the MKH model for $n''_{00} = 0.4$ ($n''_{00} = \langle \frac{1}{3}\boldsymbol{n}\cdot\boldsymbol{n}^{\alpha^2}\rangle \approx \langle\alpha^2\rangle = \frac{1}{4}$). In figures 1–3 we report data on doping dependence and spin-correlation effects found for the energy dispersion and DOS, respectively, in the SB, for the following parameter sets: $n_h = 0, n_h = 0.1$ both with $n''_{00} = 0.25$; and $n_h = 0.1$ with $n''_{00} = 0.4$ (n_h is the hole density in the p cluster). Via the first two figures we study doping from the insulator phase (figure 1) with no hole in the p cluster to the metallic phase (figure 2) with $n_h = 0.1$; whereas via figures 2, 3 we consider, for the metallic states, the effect of second-order spin–spin correlations given by the parameter n''_{00}, which

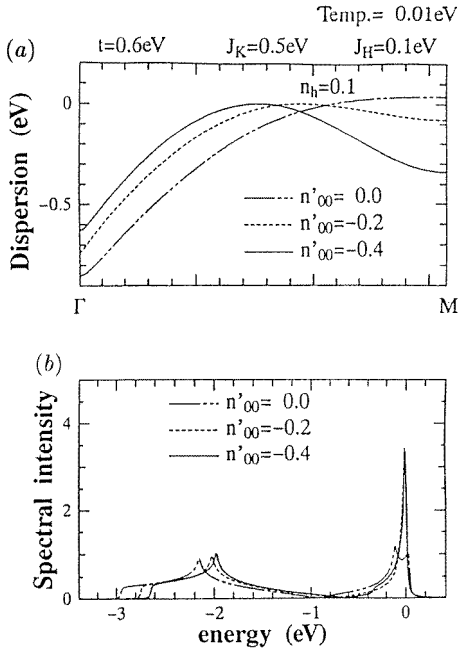

Figure 3. (*a*) The MKH dispersion energy $E_+(\boldsymbol{k})$ of the SB, and (*b*) the $\boldsymbol{k}$-integrated spectral density $\sigma_{pp}(\omega)$, both for the doped regime ($n_h = 0.1$) and for three n'_{00}-values: 0.0 (chain), -0.2 (dashed), -0.4 (line). The parameter n''_{00} is fixed at $n''_{00} = 0.4$. The temperature is $T = 0.01$ eV.

is $n''_{00} = 0.25$ in figure 2 and $n''_{00} = 0.4$ in figure 3. The chemical potential is fixed in such a way that the Fermi energy is at $\omega = 0$. Doping is given by the oxygen hole number $n_h = 2 - n - n_p$ where $n = \langle d^\dagger d \rangle$ is the d-electron density and $n_p = \langle p^\dagger p \rangle$ is the p-electron density. For these models we keep to the half-filled case for the localized spin on the copper sites in the antiferromagnetic insulator limit. Hence, at half-filling: $n = 1$ and $n_h = 0$.

A very important result is the *spin effect* on the SB dispersion energy: the strong bending of the band at the M point. This effect is induced by the strong competition between n'_{00}- and n''_{00}-contributions (see also the following discussion of the parameters from the tables). It is reduced by increasing doping, recovering to the usual free-particle-like band at $n'_{00} = 0$, and enhanced by increasing n''_{00} (above n'_{00}) up to the same order of the bandwidth as the one in figure 3(*a*) for $n''_{00} = 0.4$. As we see in all of the figures, this effect is always present in the MKH model.

As far as a comparison with experiment is concerned, the following results are essential. For fixed n''_{00}, we observe that SB pole intensities and SB bandwidths increase on increasing the doping. Moreover, for fixed doping, the bandwidth is controlled by short-range correlations given by n'_{00} and n''_{00}. *The bandwidth decreases when nearest-neighbour short-range spin correlations tend to the antiferromagnetic value.* Despite the n'_{00}-behaviour, *when n''_{00} increases, the bandwidth also increases, but with the opposite tendency with respect to n'_{00}.* It is very important also that the spin effect becomes stronger when n''_{00} increases. This means that the spin-effect increase and bandwidth decrease have different origins—respectively, one from n''_{00} and the other from n'_{00}—which are in strong competition. For the SB bandwidth at 10% hole concentration we find that the experimental value [22] of about 0.65 eV is obtained from figure 2 for $n'_{00} \sim -\frac{1}{3}$. The mean-field n'_{00} represents the

nearest-neighbour spin correlation, and its range [20, 12] is from -1 (the local singlet limit) to $\frac{1}{3}$ (the local triplet limit). In the antiferromagnetic limit, its value [20, 12] is $-\frac{1}{3}$. The experimental value of the SB bandwidth is obtained for dominant antiferromagnetic local spin coupling. This is consistent with the suggestion [18–20] that antiferromagnetic spin correlations should reduce the SB bandwidth value from the approximated calculated value to the experimental range.

Table 3. Calculated KH mean fields for fixed hole number n_h and nearest-neighbour spin correlations n'_{00}.

n_h (n'_{00})	0.01 (0.0)	0.1 (0.0)	0.01 (-0.2)	0.1 (-0.2)	0.01 (-0.4)	0.1 (-0.4)
ϵ_p	-2.2834	-2.1857	-2.1726	-2.1073	-2.0714	-2.0289
a	0.0050	0.0500	0.0050	0.0500	0.0050	0.0500
a_s	0.0111	0.1140	0.0100	0.1045	0.0093	0.10954
a'_s	-0.0105	-0.0922	-0.0093	-0.0855	-0.0075	-0.0785
a_{ss}	0.0372	0.3782	0.0350	0.3591	0.0336	0.3409
a'_{ss}	-0.0232	-0.2095	-0.0186	-0.1779	-0.0124	-0.1490

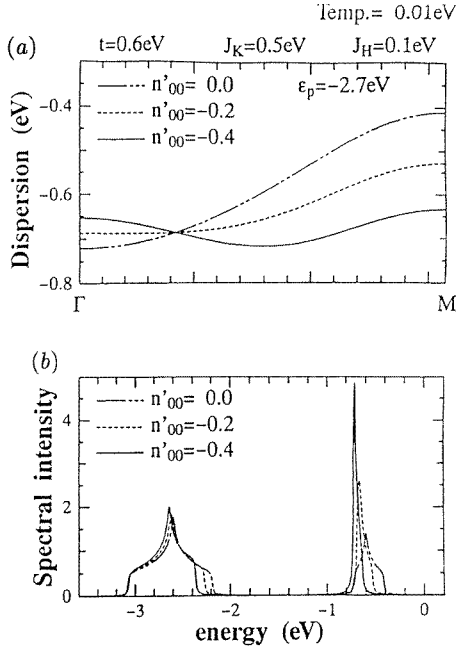

Figure 4. (*a*) The KH dispersion energy $E_+(\boldsymbol{k})$ of the SB, and (*b*) the $\boldsymbol{k}$-integrated spectral density $\sigma_{pp}(\omega)$, both for the undoped regime ($n_h = 0$ at $\epsilon_p = -2.7$ eV) and for three n'_{00}-values: 0.0 (chain), -0.2 (dashed), -0.4 (line). The temperature is $T = 0.01$ eV.

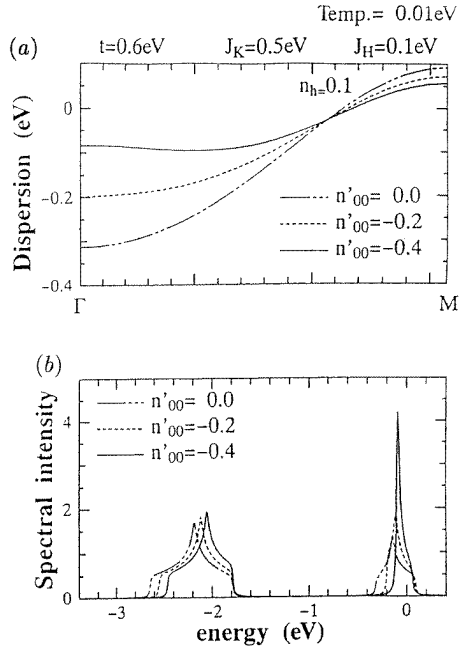

Figure 5. (*a*) The KH dispersion energy $E_+(\boldsymbol{k})$ of the SB, and (*b*) the $\boldsymbol{k}$-integrated spectral density $\sigma_{pp}(\omega)$, both for the doped regime ($n_h = 0.1$) and for three n'_{00} values: 0.0 (chain), -0.2 (dashed), -0.4 (line). The temperature is $T = 0.01$ eV.

Another result is the distribution of pole energy strengths of the TB and SB in the DOS spectrum. The SB DOS shows a distortion from the standard mean-field pole singularity. This is a typical spin-correlation effect [8, 27]. These new data show the doping and the n''_{00}-dynamics of this SB distortion, the latter also found in the p–d calculation of [20].

In the insulator, on increasing n''_{00}, the pole energy position ϵ_{SB} of the SB for $n'_{00} = 0$ moves toward the FL and increases in intensity, despite the fact that for the case where $n'_{00} \neq 0$ the intensity decreases. Observe that from the interpretation in terms of a moving chemical potential, this means that the FL moves inside the singlet band. Moreover, we also stress that TB peaks for different n'_{00}-values move far away from the FL for strong doping, producing a slight increase of the TB–SB gap. For heavy doping and increasing n''_{00}, the ϵ_{SB}-position at $n'_{00} = 0$ moves toward the ϵ_{SB}-position at $n'_{00} \neq 0$. At $n''_{00} = 0.25$ the ϵ_{SB}-position at $n'_{00} = 0$ is much further from FL than it is for $n'_{00} \neq 0$, but on increasing n''_{00} to $n''_{00} = 0.4$ the ϵ_{SB}-position goes toward the FL.

In figures 4 and 5 and table 3 we report data on the KH model, which is given by the requirements that $\gamma = 1$ and $\lambda = 0$ in all formulas of section 2. The requirement $\gamma = 1$ is to reduce the Kondo interaction at the Cu sites and $\lambda = 0$ reduces the MKH to the KH in the sense that higher-order $\boldsymbol{k}$-dependent terms via α^2, high-order copper spin–spin correlations proportional to n''_{00}, and, finally, high-order fermionic oxygen spin–spin dressed correlations given by the extended (via the α-factor) mean fields a'_{ss} are all neglected. The results are opposite, stressing the great importance of spin-cluster correlations and momentum dependence in the extended cluster for CT insulator materials. In figures 4 and 5 we report data for $n_h = 0$ and $n_h = 0.1$, respectively, for the insulator and the doped regimes. Three cases for n'_{00} show that *no spin effect* is found at the M point and a free-particle-like band form is obtained. Moreover, the SB is also shifted to higher energies, stressing the low-energy contributions of the neglected terms, and its bandwidth collapses to $\sim$0.1 eV for a 10% doping concentration. In the insulator (figure 4), the band energy is almost symmetric at the Γ and M points of the Brillouin zone, and for increasing n'_{00} the symmetry increases whereas for increasing doping it decreases—recovering the asymmetric form at $n'_{00} = 0$. On doping, the SB intensity decreases and the bandwidth increases, because the peak distortion moves towards the FL.

From table 1 we observe that all mean-field parameters proportional to the p-hole number

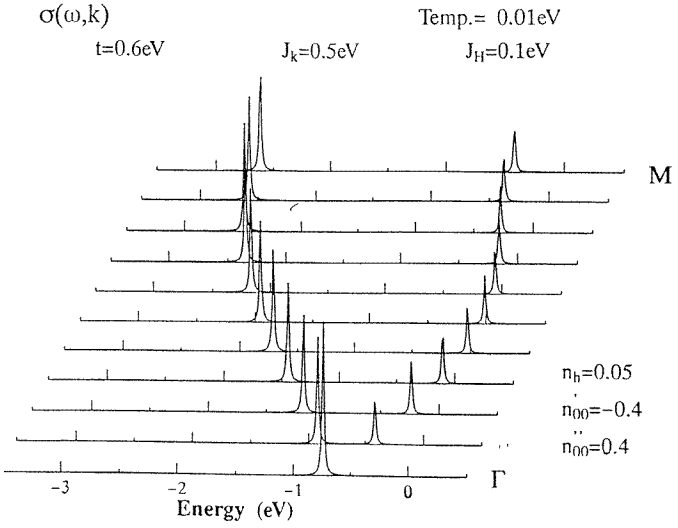

Figure 6. The MKH spectral density $\sigma_{pp}(\omega, \boldsymbol{k})$ for the doped regime ($n_h = 0.05$) with $n'_{00} = -0.4$ and $n''_{00} = 0.4$. The temperature is $T = 0.01$ eV.

(a, a_s, a_{ss}) increase on doping, whereas high-order p-hole-spin–d-electron-spin correlations (a'_s, a'_{ss}) decrease on doping. The behaviour of the same parameters is opposite for increasing nearest-neighbour d-spin correlation n'_{00}. By comparing table 1 with table 2, we can observe the effect of increasing n''_{00}: a, a_s, and a_{ss} decrease; and a'_s and a'_{ss} increase. The parameter behaviour is consistent with the expected phenomenology: hole doping destroys the strong spin–spin correlations working in the insulator at half-filling. Anyway, the incoming strong competition arising from hole doping and spin–spin correlations produces a typical frustrated spin configuration. Because of this, say, first kind of competition, the present analytical picture is very sensitive to the boson parameters n'_{00} and n''_{00}. The same complicated tendency is shown by the n'_{00_p}-operator which is proportional to $n_h n'_{00}$ for fixed n''_{00}. If n'_{00} is fixed, n'_{00_p} decreases on increasing the doping, but on increasing n''_{00} the competition becomes evident from oscillations around some constant value for high doping. Moreover, we point out that the role of the second kind of competition—of n'_{00} and n''_{00} themselves—is particularly important, inducing a change of signal going from $n'_{00} = -0.2$ to $n'_{00} = -0.4$ in the parameters a'_s and a'_{ss}, and showing that their increase is very strong and very slightly reduced by the increase of n''_{00}. This second kind of competition is responsible for the spin effect so evident in the figures. This situation is much clearer if we compare tables 1 and 2 with table 3, the latter for the KH model in which $n''_{00} = 0$. In the latter case, the qualitative behaviour of all parameters agrees with the MKH picture, but a'_s and a'_{ss} keep the same sign, and therefore increase very slowly, until finally there is no spin effect on the band. The spin effect is the result of the so-called second kind of competition given by the Kondo-type interaction for the *extended cluster*. Thus we expect that, in a self-consistent calculation of fermion and boson parameters [12], the two boson parameters n'_{00} and n''_{00} will very strongly contribute in the search for the fixed point.

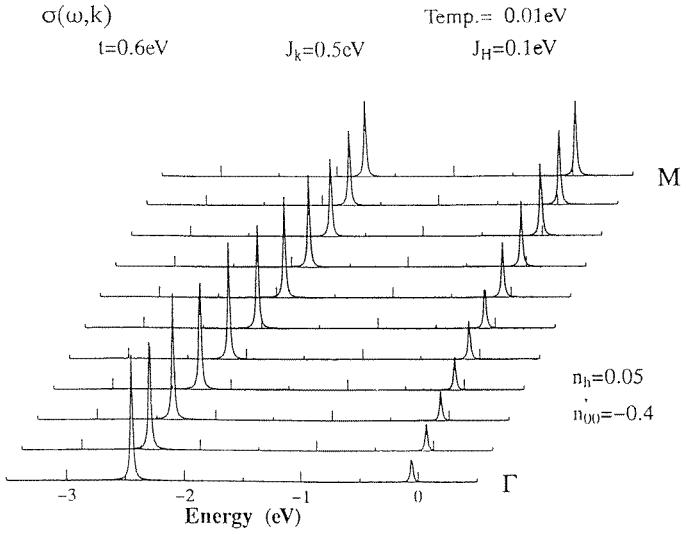

Figure 7. The KH spectral density $\sigma_{pp}(\omega, \boldsymbol{k})$ for the doped regime ($n_h = 0.05$) with $n'_{00} = -0.4$. The temperature is $T = 0.01$ eV.

In figures 6 and 7 we report the $(\omega, \boldsymbol{k})$-dependences of the MKH and KH DOS, respectively, for the following parameter values: $n_h = 0.05, n'_{00} = -0.4, n''_{00} = 0.4$; and $n_h = 0.05, n'_{00} = -0.4$. The MKH spectrum shows the bending at the M point of the SB

while the KH one is almost flat. The TB in the MKH case has the opposite form to and also a larger bandwidth than the KH case.

4. Concluding remarks

Antiferromagnetic spin correlations have been investigated in the MKH model up to second order (two dashes on the boson parameter). The results demonstrate the importance of the competition of two kinds of short-range antiferromagnetic correlation: nearest-neighbour (n'_{00}) and next-to-nearest-neighbour (n''_{00}) spin correlations on copper sites.

For a normal-phase high-T_c oxide superconductor we assume that the main excitations from a paramagnetic ground state (i.e. no chiral states) and near the Fermi level are given by thermal collective states produced by energy level mixing of bare states introduced by the special choice of basic composite fields. The approximations in the calculation are given by the expansion of high-order operators in terms of a fixed operator basis which is defined by the physics around the Fermi level. The energies of the p_γ and p_s levels are nearly the same, and are comparable with the Fermi energy.

No other calculation has been done for the IMT in an effort to understand the details of the singlet band in MKH models. In [9, 10] only one–two-hole motion is considered, and the existence of the transition is pointed out with the singlet formation roughly at reasonable expected energies. True comparisons can only be with analogous results reported for the parent p–d model.

The width calculation of the singlet-type band crossing the Fermi level for a 10% doping concentration predicts the experimental value very well. In fact, we can reduce the previous theoretical bandwidth predictions [19, 20] to the experimental value [22] by triggering n'_{00} and n''_{00}. This bandwidth is strongly reduced by the nearest-neighbour spin correlations when n'_{00} decreases to the antiferromagnetic value, and it increases if n''_{00} increases. n''_{00} is not explicitly controlled in the p–d model calculations [19, 20].

A spin effect on the band dispersion is observed, and is described for a large set of parameter values. The spin effect is also produced by the boson parameters n'_{00} and n''_{00} which are defined by the complex Kondo-type interactions on the extended clusters in the MKH model. For sufficiently extended clusters, n''_{00} contributes together with n'_{00} to increase the spin effect. When the Kondo interaction is reduced only at the Cu sites, the KH model no longer shows a spin effect, and the singlet-type bandwidth collapses to $\sim$0.1–0.2 eV, far from the experimental data. The same spin effect is reported for the first time in the p–d model [20] but involved in the complex spin–charge composite p–d interactions in which the contribution from n''_{00} is not manifest. In [19] the spin effect is not observed at all, probably because of the finite-U, Coulomb on-site repulsion, and therefore more complex (than those considered in [20]) p–d cluster-renormalized interactions from the lower-Hubbard-level transitions.

We have restricted our calculation to the mean-field limit of the composite-operator approach to the MKH model (see after equation (2.10)). The self-energy contributions ω and $\boldsymbol{k}$ from $\delta m(\omega, \boldsymbol{k})$ in equation (2.10) have never been considered in previous calculations for MKH models. However, in the p–d model [22], $\delta m_{pp}(\boldsymbol{k})$ has been estimated for a generalized one-loop composite-operator approximation [23, 24, 12] to the self-energy contribution for the singlet band. The correction goes in the same direction as the one from n''_{00}, i.e. it enlarges the bandwidth. In fact the loop correction is an intersite contribution which carries indirect cluster correlations related to n''_{00}. As we have seen, in the MKH model, the mean-field result is enough for estimating the singlet bandwidth, but most importantly it clarifies the physical role of n''_{00}. Thus, we expect a complicated

dynamical decay of composite-operator quasi-particles in a self-consistent treatment of n''_{00} including dynamical corrections (work in progress), as was suggested by results in [23] (see also [27]), where the imaginary part of the self-energy (the ω-dependence) of the electron vanishes at $\omega = 0$ ($T = 0$) and starts increasing with ω—behaviour which is given by the only spin-fluctuation contribution, from n'_{00}.

The two phenomena predicted—the W_s-bandwidth contraction and the spin effect—have different origins: (a) the bandwidth decreases on decreasing n'_{00} and increases on increasing n''_{00}; and (b) the spin effect increases on decreasing n'_{00} and is also enhanced on increasing n''_{00}. Therefore, the spin effect increase 'works' for W_s-bandwidth reduction and it is mainly *produced* by n'_{00}, while bandwidth reduction is *controlled and suppressed* by n''_{00}. Antiferromagnetic local spin correlations have strong effects in the MKH model because of the first-order role played by the next-to-nearest-neighbour spin correlations (given by n''_{00}). A typical frustration mechanism [14–16] seems to exist into the extended clusters and it is generated, on the one hand, by the hole-doping–spin-interaction competition, and, on the other hand, by the nearest-neighbour–next-to-nearest-neighbour spin competition. Frustration has been mainly considered only in the superexchange interaction Cu–O–Cu ligand spins, and, therefore, for the Cu nearest neighbours [14, 15, 13]. However, high-order terms in spin–spin correlations have been discussed [16] for the Inui, Doniach and Gabay effective model in which a Heisenberg antiferromagnet is weakly doped, and it is found that second and third neighbours depend directly on doping implementing strong frustration effects on the stiffness and velocity of spin waves.

Acknowledgments

The authors would like to thank to Professor M Tachiki, Dr T Koyama, Dr S Takahashi and Mr S Ishihara for useful discussions. This work was supported by a Grant in Aid from the Ministry of Education, Japan. One of the authors (AMA) was supported by a Grant in Aid for Scientific Research of the Special Exchange Programme from the Japanese–German Centre, Berlin (JGCB), and is grateful to Mr R Biasi for kind hospitality.

Appendix A. Derivation of Hamiltonian parameters of the MKH effective model from p–d model ones

To approximate p–d composite excitations to the main contributions around the FL we introduce a recursive iteration by using Taylor expansion of composite operators to identify each order of the expansion by the effective couplings.

Let us start from p–d equations of motion presented in detail in [20]:

$$\mathrm{i}\frac{\partial}{\partial t}p = \epsilon_p p + 2t_0\eta_\gamma \tag{A.1}$$

$$\mathrm{i}\frac{\partial}{\partial t}\eta = \epsilon_\eta \eta - t_0\sigma^\mu n_\mu p_\gamma. \tag{A.2}$$

The Fourier transform of equation (A.2) is

$$\eta = -\frac{t_0}{(\omega - \epsilon_\eta)}\sigma^\mu n_\mu p_\gamma. \tag{A.3}$$

To pick up the energy components of (A.3) around $\omega \sim \epsilon_p$, we can write the ω-function as

$$\frac{1}{\omega - \epsilon_\eta} = \frac{1}{(\omega - \epsilon_\eta) - (\epsilon_\eta - \epsilon_p)}. \tag{A.4}$$

The Taylor expansion of (A.4) around $\omega \sim \epsilon_p$ is

$$\frac{1}{(\omega - \epsilon_\eta)} = -\frac{1}{(\epsilon_\eta - \epsilon_p)}\left(1 + \frac{\omega - \epsilon_p}{(\epsilon_\eta - \epsilon_p)}\right) + \cdots. \tag{A.5}$$

At first order of the (A.5) expansion, we have from equation (A.3)

$$\eta \simeq \frac{t_0}{(\epsilon_\eta - \epsilon_p)}\sigma^\mu n_\mu p_\gamma. \tag{A.6}$$

By inserting (A.6) into equation (A.1) we have

$$\mathrm{i}\frac{\partial}{\partial t}p = \epsilon_p p + \frac{2t_0^2}{(\epsilon_\eta - \epsilon_p)}(\sigma^\mu n_\mu p_\gamma)^\gamma \tag{A.7}$$

which for $\mu = 0$ defines the energy transfer coupling in the kinetic term of the MKH model for the p electron:

$$t = -\frac{2t_0^2\langle n\rangle}{(\epsilon_\eta - \epsilon_p)}. \tag{A.8}$$

At second order of the (A.5) expansion, we have from equation (A.3)

$$\eta = \frac{t_0}{(\epsilon_\eta - \epsilon_p)}\sigma^\mu n_\mu \left[p_\gamma + \frac{1}{(\epsilon_\eta - \epsilon_p)}(\omega - \epsilon_p)p_\gamma\right] \tag{A.9}$$

and since the Fourier transform of equation (A.1) is

$$p = \frac{2t_0}{(\omega - \epsilon_p)}\eta_\gamma \tag{A.10}$$

equation (A.9) becomes

$$\eta = \frac{t_0}{(\epsilon_\eta - \epsilon_p)}\sigma^\mu n_\mu \left[p_\gamma + \frac{1}{(\epsilon_\eta - \epsilon_p)}(2t_0)\eta_{\gamma^2}\right]. \tag{A.11}$$

Therefore, by using again the first-order approximation,

$$\eta = \frac{t_0}{(\epsilon_\eta - \epsilon_p)}\sigma^\mu n_\mu \left[p_\gamma + \frac{1}{(\epsilon_\eta - \epsilon_p)}\frac{(2t_0^2)}{(\epsilon_\eta - \epsilon_p)}(\sigma^\mu n_\mu p_\gamma)_{\gamma^2}\right]. \tag{A.12}$$

Finally, to calculate the two coupling constants of the MKH model related to spin couplings, we consider the equation of motion for fluctuations from the p–d model:

$$\mathrm{i}\frac{\partial}{\partial t}n_\mu = 2t_0(\eta^\dagger\sigma_\mu p_\gamma - p_\gamma^\dagger\sigma_\mu\eta). \tag{A.13}$$

Let us remember that the MKH model is derived [8] assuming n_0 constant (no charge fluctuations). At half-filling we have $n_0 \equiv \langle n\rangle = 1$. From equations (A.12) and (A.13), both for the spin component, we find

$$\mathrm{i}\frac{\partial}{\partial t}n_i = \frac{4t_0^2}{(\epsilon_\eta - \epsilon_p)}\mathrm{i}\epsilon_{ijk}p_\gamma^\dagger\sigma_i p_\gamma n_k + \frac{8t_0^4}{(\epsilon_\eta - \epsilon_p)^3}\langle p^\dagger p^{\alpha 2}\rangle\mathrm{i}\epsilon_{ijk}n_j^\alpha n_k \tag{A.14}$$

where we can identify the Kondo term in the first term and the Heisenberg one in the second term—whose coefficients are, respectively, the Kondo and Heisenberg couplings from the p–d model.

At half-filling, from equations (A.8) and (A.14) we have for the MKH model

$$t = -\frac{2t_0^2}{(\epsilon_\eta - \epsilon_p)}$$
$$J_k = \frac{2t_0^2}{(\epsilon_\eta - \epsilon_p)} \tag{A.15}$$
$$J_H \equiv 4J = \frac{t_0^4}{(\epsilon_\eta - \epsilon_p)^3}.$$

In this paper we consider the following realistic parameters: $t_0 = 0.6$ eV and $\Delta = (\epsilon_\eta - \epsilon_p) = 1.2$ eV. The related MKH values from equation (A.15) are $|t| = 0.6$ eV, $J_k = 0.5$ eV, and $J = 0.025$ eV or $J_H = 0.1$ eV. The sign of t depends on the sign definition in the MKH Hamiltonian. In equation (2.1) we define t to be positive.

Appendix B. The composite-operator method

In the composite-operator method [23], excitation modes are identified by choosing a certain series of operators (generally composite) and by expanding the time derivative of operators in terms of this operator series. To define the expansion, the normalization matrix must be identified and then the expansion coefficients are identified.

Let us assume that we have identified an appropriate series of fermionic operators $\psi_n(\boldsymbol{x})$. Their time derivatives are expressed as an expansion in terms of this series of operators and residual terms:

$$\mathrm{i}\frac{\partial}{\partial t}\psi_n(x) = \sum_{n'} \epsilon_{nn'}(-\mathrm{i}\boldsymbol{\nabla})\psi_{n'}(x) + \delta j_n(x) = j_n(x) \tag{B.1}$$

where x indicates $(t, \boldsymbol{x})$ and $\epsilon_{nn'}(-\mathrm{i}\boldsymbol{\nabla})$ indicates that the coefficients $\epsilon_{nn'}$ operate as the momentum-dependent $\epsilon_{nn'}(\boldsymbol{k})$ on the Fourier transform of $\psi_n(x)$. For the normalization of operators, we use the norm

$$I_{nl}(\boldsymbol{k}) = \mathrm{FT}\langle\{\psi_n(\boldsymbol{x}), \psi_l^\dagger(\boldsymbol{y})\}\rangle \tag{B.2}$$

where FT indicates the Fourier transform and is defined for an arbitrary function $f(\boldsymbol{x})$ as

$$\mathrm{FT}f(\boldsymbol{x}) = \int \mathrm{d}^2x\ \mathrm{e}^{-\mathrm{i}\boldsymbol{k}\cdot\boldsymbol{x}} f(\boldsymbol{x}). \tag{B.3}$$

The expansion coefficients are defined from

$$m_{nl}(\boldsymbol{k}) \equiv \sum_{l'} \epsilon_{nl'}(\boldsymbol{k}) I_{l'l}(\boldsymbol{k}) = \mathrm{FT}\langle\{j_n(\boldsymbol{x}), \psi_l^\dagger(\boldsymbol{y})\}\rangle \tag{B.4}$$

with

$$\langle\{\delta j_n(\boldsymbol{x}), \psi_l^\dagger(\boldsymbol{y})\}\rangle = 0. \tag{B.5}$$

In the present model and for the present basis (2.4) this condition is verified (for details see [3] and [9]). The coefficients $\epsilon_{nl}(\boldsymbol{k})$ are mean fields which represent the level shift and the on-site and intersite mixing among composite excitations. The matrix $m_{nl}(\boldsymbol{k})$ has the hermiticity property:

$$m_{nl}(\boldsymbol{k}) = m_{ln}(\boldsymbol{k})^* \tag{B.6}$$

since

$$\left\langle\left\{\mathrm{i}\frac{\partial}{\partial t}\psi_n(\boldsymbol{x}), \psi_l^\dagger(\boldsymbol{y})\right\}\right\rangle = \left\langle\{\psi_n(\boldsymbol{x}), -\mathrm{i}\frac{\partial}{\partial t}\psi_l^\dagger(\boldsymbol{y})\}\right\rangle. \tag{B.7}$$

Then the retarded function $\langle R\psi_n(x)\psi_l^\dagger(y)\rangle$ is obtained in the form

$$\mathrm{FT}\langle R\psi_n(x)\psi_l^\dagger(y)\rangle = \left(\frac{1}{\omega - \epsilon(\boldsymbol{k}) - \Sigma(\omega,\boldsymbol{k})} I(\boldsymbol{k})\right)_{nl} \tag{B.8}$$

where FT again indicates the Fourier transform and is now defined by

$$\mathrm{FT}\langle R\psi_n(x)\psi_l^\dagger(0)\rangle = -\mathrm{i}\int \mathrm{d}t\ \mathrm{d}^2x\ \mathrm{e}^{\mathrm{i}\omega t - \mathrm{i}\boldsymbol{k}\cdot\boldsymbol{x}}\langle R\psi_n(x)\psi_l^\dagger(0)\rangle. \tag{B.9}$$

The self-energies $\Sigma(\omega,\boldsymbol{k})$ and $\Sigma^\dagger(\omega,\boldsymbol{k})$ are defined by

$$\langle R\,\delta j_n(x)\,\psi_l^\dagger(y)\rangle = \sum_{n'}\Sigma_{nn'}\left(\mathrm{i}\frac{\partial}{\partial t}, -\mathrm{i}\boldsymbol{\nabla}\right)\langle R\psi_{n'}(x)\psi_l^\dagger(y)\rangle \tag{B.10a}$$

and

$$\langle R\psi_n(x)\,\delta j_l^\dagger(y)\rangle = \sum_{l'}\langle R\psi_n(x)\psi_{l'}^\dagger(y)\rangle\Sigma_{l'l}^\dagger\left(-\mathrm{i}\frac{\partial}{\partial t_y}, \mathrm{i}\boldsymbol{\nabla}_y\right). \tag{B.10b}$$

They are obtained from

$$\delta m_{nl}(\omega,\boldsymbol{k}) \equiv \mathrm{FT}\langle R\,\delta j_n\,\delta j_l^\dagger\rangle_I = \Sigma(\omega,\boldsymbol{k})I(\boldsymbol{k}) = I(\boldsymbol{k})\Sigma^\dagger(\omega.\boldsymbol{k}) \tag{B.11}$$

where the subscript 'I' indicates the irreducible part, and from equations (B.8) and (B.10) is defined by

$$\langle R\,\delta j_n(x)\,\delta j_l^\dagger(y)\rangle_I = \langle R\,\delta j_n(x)\,\delta j_l^\dagger(y)\rangle - \sum_{l'}\Sigma_{l'l}^\dagger\left(-\mathrm{i}\frac{\partial}{\partial t_y}, \mathrm{i}\boldsymbol{\nabla}_y\right)\langle R\,\delta j_n(x)\,\psi_{l'}^\dagger(y)\rangle. \tag{B.12}$$

The dynamical correction $\delta m(\omega,\boldsymbol{k})$ satisfies the sum rule

$$\int \mathrm{d}\omega\ \left(-\frac{1}{\pi}\right)\mathrm{Im}\,\delta m_{nl}(\omega,\boldsymbol{k}) = \mathrm{FT}\langle\{\delta j_n(\boldsymbol{x}), \delta j_l^\dagger(\boldsymbol{y})\}\rangle. \tag{B.13}$$

References

[1] 1994 *Proc. 4th Int. Conf. on M^{2}S-HTSC (Grenoble, 1994); Physica* C **235–240**
[2] Bulaevskii L N, Nagaev E L and Khomskii D L 1968 *Sov. Phys.–JETP* **27** 1562
Brinkman W F and Rice T M 1970 *Phys. Rev.* B **2** 1324
Shraiman B I and Siggia E D 1988 *Phys. Rev. Lett.* **60** 740
Schmitt-Rink S, Varma C M and Ruckenstein A E 1988 *Phys. Rev. Lett.* **60** 2793
[3] Igarashi J and Fulde P 1992 *Phys. Rev.* B **45** 10 419, 12 357
[4] Igarashi J and Fulde P 1993 *Phys. Rev.* B **48** 998
[5] Wrobil P and Eder R 1994 *Phys. Rev.* B **49** 1233
[6] Prelovsek P 1988 *Phys. Lett.* **126A** 287
Fukuyama H, Matsukawa H and Hasegawa Y 1989 *J. Phys. Soc. Japan* **58** 364
Furukawa N and Imada M 1990 *J. Phys. Soc. Japan* **59** 1771
[7] Emery V J and Reiter G 1988 *Phys. Rev.* B **38** 4547, 11 938
Zaanen J and Oleś A M 1988 *Phys. Rev.* B **37** 9423
Schüttler H B and Fedro A J 1988 *J. Appl. Phys.* **63** 4209
[8] Ishihara S, Matsumoto H and Tachiki M 1990 *Phys. Rev.* B **42** 10 041
[9] Loh E Y Jr, Martin T, Prelovsek P and Campbell D K 1988 *Phys. Rev.* B **38** 2494
Frenkel D M, Gooding R J, Shraiman B I and Siggia E D 1990 *Phys. Rev.* B **41** 350
Stephan W and Horch P 1991 *Phys. Rev. Lett.* **66** 2258
[10] Chen C-X, Schüttler H-B and Fedro A J 1990 *Phys. Rev.* **41** 2581
[11] Matsumoto H, Allega A M, Odashima S and Mancini E F 1994 *Physica* C **235–240** 2227
[12] See
Allega A M 1995 *PhD Thesis* University of Salerno

for a systematic formulation of the method, including a preliminary version of a self-consistent calculational scheme for bosons and dynamical corrections, with a collection of applications, e.g. on the pure Heisenberg $D = 2$ model; see also
Allega A M, Odashima S, Matsumoto H and Mancini E F 1994 *Physica* C **235–240** 2229
[13] Ko D Y K 1990 *Phys. Rev. Lett.* **65** 16
Scherman A and Schreiber M 1993 *Phys. Rev.* B **48** 7492
[14] Pimentel J R and Orbach R 1992 *Phys. Rev.* B **46** 2920
[15] Aharony A, Birgeneau R J, Coniglio A, Kastner M A and Stanley H E 1988 *Phys. Rev. Lett.* **60** 1330
[16] Birgeneau R J, Kastner M A and Aharony A 1988 *Z. Phys.* B **71** 57
[17] Jolicoeur T and Guillou J C 1989 *Europhys. Lett.* **10** 599
[18] Unger P and Fulde P 1993 *Phys. Rev.* B **47** 8947
[19] Unger P and Fulde P 1993 *Phys. Rev.* B **48** 16 607
[20] Ishihara S, Matsumoto H, Odashima S, Tachiki M and Mancini F 1994 *Phys. Rev.* B **49** 1350
[21] Emery V J 1987 *Phys. Rev. Lett.* **58** 2794
[22] Fink J, Nücker N, Romberg H, Alexander M, Adelman P, Claessen R, Mante G, Buslaps T, Harm S, Manzke R E and Skibowsky 1991 *Highlights in Condensed Matter Physics and Future Prospects* ed G L Esaki (New York: Plenum)
[23] Matsumoto H, Sasaki M, Ishihara S and Tachiki M 1992 *Phys. Rev.* B **46** 3009
Sasaki M, Matsumoto H and Tachiki M 1992 *Phys. Rev.* B **46** 3022
[24] Matsumoto H, Allega A M and Odashima S 1994 Composite operator method for strongly correlated electron systems *Superconductivity and Strongly Correlated Electron Systems, Proc. Amalfi Int. Conf. (Italy)* ed C Noce, A Romano and G Scarpetta (Singapore: World Scientific) p 93
[25] Mancini F, Marra S, Allega A M and Matsumoto H 1994 Analysis of the Hubbard model by composite operator method in a generalized mean field approximation *Superconductivity and Strongly Correlated Electron Systems, Proc. Amalfi Int. Conf. (Italy)* ed C Noce, A Romano and G Scarpetta (Singapore: World Scientific) p 271
[26] Marra S, Mancini F, Allega A M and Matsumoto H 1994 *Physica* C **235–240** 2253
[27] Matsumoto H, Ishihara S and Tachiki M 1992 *J. Phys. Chem. Solids* **53** 1507